LA-UR- 02- 824

Approved for public release;
distribution is unlimited.

Title: Photonuclear Physics in Radiation Transport:
I. Cross Sections and Spectra

Author(s): M. B. Chadwick, P. G. Young, and R. E MacFarlane, T-16
M. C. White and R. C. Little, X-5

Submitted to: Nuclear Science and Engineering

LOS ALAMOS NATIONAL LABORATORY
3 9338 00854 8231

Los Alamos
NATIONAL LABORATORY

Los Alamos National Laboratory, an affirmative action/equal opportunity employer, is operated by the University of California for the U.S. Department of Energy under contract W-7405-ENG-36. By acceptance of this article, the publisher recognizes that the U.S. Government retains a nonexclusive, royalty-free license to publish or reproduce the published form of this contribution, or to allow others to do so, for U.S. Government purposes. Los Alamos National Laboratory requests that the publisher identify this article as work performed under the auspices of the U.S. Department of Energy. Los Alamos National Laboratory strongly supports academic freedom and a researcher's right to publish; as an institution, however, the Laboratory does not endorse the viewpoint of a publication or guarantee its technical correctness.

Form 836 (8/00)

LA-UR-02-824

Photonuclear physics in radiation transport: I. Cross sections and spectra

M.B. Chadwick, P.G. Young, and R.E. MacFarlane

Theoretical Division, University of California,

Los Alamos National Laboratory, Los Alamos, NM 87545

M.C. White and R.C. Little

X-Division, University of California,

Los Alamos National Laboratory, Los Alamos, NM 87545

Abstract

We describe model calculations and nuclear data evaluations of photonuclear reactions on isotopes of C, O, Al, Si, Ca, Fe, Cu, Ta, W, and Pb, for incident photon energies up to 150 MeV. The calculations, using the GNASH code, include Giant Dipole Resonance and quasideuteron models for photoabsorption. The emission of secondary particles and gamma-rays are computed using preequilibrium theory, together with an open-ended sequence of compound nucleus decays using the Hauser-Feshbach theory. The accuracy of the calculated and evaluated cross sections are assessed through extensive comparisons with measured cross sections, average neutron multiplicities, and energy-dependent emission spectra. The evaluated ENDF files facilitate radiation transport studies of the importance of photonuclear reactions in a number of technologies including: photoneutrons produced in electron/photon accelerators; shielding studies; and nondestructive detection of nuclear materials. In a subsequent back-to-back paper we describe developments to the

MCNP and MCNPX codes to utilize these data in transport simulations.

I. INTRODUCTION

Photonuclear physics has, until recently, remained a strangely-neglected subject of study in radiation transport computations. Evaluated nuclear data files (ENDF), such as the U.S. ENDF/B-VI cross section library [1], have not included evaluated photonuclear cross section data, and additionally radiation transport codes have not been developed to utilize such ENDF data except for certain ad-hoc studies [2,3]. Whilst it is true that photoneutrons typically provide only a small additional neutron source in technologies involving the nuclear force (*e.g.* fission, fusion, and high-energy proton accelerator-driven spallation sources), photoneutrons are of significant importance in technologies involving electron accelerators and bremsstrahlung targets. In these cases, neutrons are produced primarily through the photonuclear reaction process, and can pose a serious concern for radiation protection and shielding. Of course, photonuclear reactions are also widely used as spallation neutron sources for physics experiments, such as the ORELA facility at Oak Ridge National Laboratory.

We present two back-to-back papers describing work at Los Alamos National Laboratory to develop a photonuclear capability in radiation transport simulations. This first paper describes our evaluation methods, including nuclear model calculations, used to produce evaluated cross section data files in the ENDF format. Results are presented for photons with incident energies up to 150 MeV on twelve isotopes of the following elements: C, O, Al, Si, Ca, Fe, Cu, Ta, W, and Pb. These represent some of the most important materials used in accelerator components, collimators and beam-shaping devices, beam-stops, bremsstrahlung conversion targets, shielding, as well as elements abundant in human tissue. In the second paper, we describe extensions to the MCNP and MCNPX radiation transport codes to utilize these photonuclear data in fully-coupled radiation transport calculations. The second paper [4] also includes some validation tests, as well as comparisons with integral experiments, to benchmark the new photonuclear capability. Earlier versions of this work have been published in a conference proceedings [5].

There are two principal reasons why photonuclear capabilities have not previously been included in transport codes through use of ENDF files: (1) Experimental photonuclear data from different laboratories (*e.g.* data from the measurement programs at Livermore, Saclay, and Illinois) often show discrepancies that must be resolved in the evaluation procedure; and (2) There are few measurements of the energy- and angle-dependent spectra of secondary particles emitted in photonuclear reactions. Most of the existing spectral measurements are for bremsstrahlung photon sources, instead of for monoenergetic sources as required for a complete cross section evaluation. Because a radiation transport code needs such energy spectra information, some of the most widely-used photonuclear data compilations, such as those of Dietrich and Berman [6] and Varlamov *et al.* [7], are not immediately usable in a transport context. The present work largely depends upon nuclear model calculations to estimate emission spectra, though these calculated spectra are consistently obtained together with the calculated cross sections for various channels, *e.g.* $(\gamma, 1n)$, $(\gamma, 2n)$, *etc.*, that can be validated through comparisons with measured values.

A number of other researchers from laboratories in Japan (JAERI, Tokai), South Korea (KAERI, Taejon), Russia (IPPE, Obninsk and Moscow State University), China (CIAE, Beijing), and Brazil (University of Sao Paulo) are presently working on the development of photonuclear reaction cross section data for transport applications, under the coordination of an International Atomic Energy Agency (IAEA) Coordinated Research Project (CRP), entitled "Compilation and Evaluation of Photonuclear Data for Applications" [8]. The present work is part of this effort, and a full suite of ENDF evaluations for over 160 isotopes will be released in 2000 on a compact disc (CD) together with documentation in an IAEA report [9]. The following photonuclear applications were of primary concern to this project: (a) Photoneutrons produced in medical electron accelerators used in cancer radiotherapy, for radiation protection and dosimetry applications, and the impact of photoneutrons and photoprotons on absorbed dose in the body; (b) Detection of nuclear materials (*e.g.* actinides) using nondestructive remote detection of photoneutrons, or characteristic decay gamma-rays, following photonuclear reactions induced by photons produced by a compact electron

accelerator or other sources; (c) Activation analyses for the production and transmutation of isotopes in a photon field; (d) Plasma diagnostics in fusion technologies; (e) Nuclear astrophysics, where photonuclear reactions play an important role in stellar nucleosynthesis.

While this paper is the first work to present photonuclear reaction analyses in the ENDF format, for use in radiation transport simulations, it is important to note that previous works have included photonuclear reactions into transport simulation codes. These intranuclear cascade codes compute the photonuclear reactions "on the fly" during the simulation. The works of Alsmiller *et al.* [10], Gabriel [11], Fasso, Ferrari and Sala [12,13], and Mokhov *et al.* [14] are particularly noteworthy. Our present approach has the advantage that one can aim to have the most accurate possible representation of the reactions, obtained from both experimental data and model calculations, in the ENDF file. (We note, though, that Fasso's approach [13] is also able to utilize experimental information). The intranuclear cascade codes have historically had the advantage that they can be used to compute photonuclear reactions on any target material, whereas transport codes that use ENDF data files are dependent upon an evaluation existing for the materials of interest. But this advantage is no longer an issue – the present work describes just twelve ENDF files for high-priority materials in accelerator technologies, but the aforementioned IAEA project will soon be issuing similar ENDF files for over 160 isotopes, which will be sufficient for essentially all applications.

This paper is organized as follows. Section II describes the nuclear models we use to compute photonuclear cross sections within the GNASH code. This includes photoabsorption reaction mechanisms, as well as preequilibrium and equilibrium emission mechanisms. A model for the angular distributions of the ejectiles is also provided. Some comparisons with measured data are given to illustrate the physics involved. Section III summarizes the ENDF formats we use to represent the cross section data, and describes developments that have been made to the NJOY code, for processing the data into a form usable by radiation transport simulation codes. Section IV presents our results, including descriptions of evaluation procedures, and shows figures of the important photonuclear cross sections compared

with measured data for validation purposes. Our conclusions are given in Section IV.

II. NUCLEAR MODEL CALCULATIONS

IIA. Photoabsorption Model

A model of photonuclear reactions must account for the different nuclear reaction mechanisms involved in the initial photonuclear excitation process, and the subsequent decay of the excited nucleus by particle and gamma-ray emission. At low energies, below about 30 MeV, the Giant-Dipole Resonance (GDR) is the dominant excitation mechanism, where a collective bulk oscillation of the neutrons against the protons occurs. At higher energies up to approximately 150 MeV, where the wavelength of the photon decreases, the phenomenological model of photoabsorption on a neutron-proton (quasi-deuteron (QD)), which has a large dipole moment, becomes important.

Models of photonuclear reactions typically begin with a determination of the photoabsorption cross section, and this can be done in one of two ways: (1) An evaluation based on experimental data, if data exist; and (2) A model calculation of photoabsorption. These methods are discussed in more detail below.

If experimental data exist for the total photoabsorption cross section, they can be used as input into most codes which model the subsequent particle emission reactions. The most useful type of experimental data here are from photon absorption experiments which measure the total photoabsorption cross section. For heavy nuclei, compilations of photoneutron total cross section such as that of Dietrich and Berman [6] can be used to approximate the photoabsorption cross sections, since contributions from photoproton reactions (and other reactions producing complex charged particles) are suppressed by the Coulomb barrier. However, in light nuclei this approach cannot be used since the photoproton cross section is no longer small, and in some cases exceeds the photoneutron cross section.

An alternative way to obtain the photoabsorption cross section is to calculate it theoret-

ically as a sum of two components [15],

$$\sigma_{abs}(\epsilon_\gamma) = \sigma_{GDR}(\epsilon_\gamma) + \sigma_{QD}(\epsilon_\gamma), \tag{1}$$

discussed in more detail below.

The GDR component, $\sigma_{GDR}(\epsilon_\gamma)$, is given by a Lorentzian shape, with parameters describing the total absorption of the giant dipole resonance. A relation to be used reads

$$\sigma_{GDR}(\epsilon_\gamma) = \sum_i \sigma_i / \left[1 + (\epsilon_\gamma^2 - E_i^2)^2 / \epsilon_\gamma^2 \Gamma_i^2\right] \tag{2}$$

where $i = 1$ for spherical nuclei, and $i = 1, 2$ for deformed nuclei which can generally be better represented as a sum of two Lorentzians, one for each axis of deformation. E_i is the position of the GDR peak, Γ_i is the GDR width, and σ_i is the peak of the resonance cross section, for Lorentzian i.

The QD component, $\sigma_{QD}(\epsilon_\gamma)$, is taken from the model of Ref. [15], which uses a Levinger-type theory. It relates the nuclear photoabsorption cross section to the experimental deuteron photodisintegration cross section $\sigma_d(\epsilon_\gamma)$,

$$\sigma_{QD}(\epsilon_\gamma) = L \, \frac{NZ}{A} \, \sigma_d(\epsilon_\gamma) \; f(\epsilon_\gamma). \tag{3}$$

Here, the Levinger parameter was derived to be $L = 6.5$ [15], and $f(\epsilon_\gamma)$ is the Pauli-blocking function, which reduces the free deuteron cross section $\sigma_d(\epsilon_\gamma)$ to account for Pauli-blocking of the excited neutron and proton by the nuclear medium. The experimental deuteron photodisintegration cross section was parameterized as

$$\sigma_d(\epsilon_\gamma) = 61.2(\epsilon_\gamma - 2.224)^{3/2} / \epsilon_\gamma^3 \text{mb}. \tag{4}$$

The Pauli-blocking was derived to be a multidimensional integral whose solution could be well approximated in the energy range $20 - 140$ MeV by the polynomial expression

$$f(\epsilon_\gamma) = 8.3714 \times 10^{-2} - 9.8343 \times 10^{-3} \epsilon_\gamma + 4.1222 \times 10^{-4} \epsilon_\gamma^2$$

$$- 3.4762 \times 10^{-6} \epsilon_\gamma^3 + 9.3537 \times 10^{-9} \epsilon_\gamma^4. \tag{5}$$

In Ref. [15] the Pauli-blocking function was not parameterized below 20 MeV, where it tends to zero, or above 140 MeV, where it tends to unity. Still, as the contribution needs to be defined at all energies considered, we use an exponential shape $f(\epsilon_\gamma) = \exp(-D/\epsilon_\gamma)$ for energies below 20 MeV, and above 140 MeV, with $D = -73.3$ for $\epsilon_\gamma < 20$ MeV and $D = 24.2$ for $\epsilon_\gamma > 140$ MeV. This form has the correct behavior in that it tends to zero at $\epsilon_\gamma = 0$, and unity for large ϵ_γ and is continuous with Eq. (5) at 20 and 140 MeV.

Photoabsorption calculations using the above model are common [16,17,12,18]. In some cases, authors have treated the Levinger parameter as an adjustable parameter to obtain best agreement with measurements in the 50 - 150 MeV photon energy region.

Finally, we note a method sometimes used by evaluators to infer the total absorption cross sections when no measured data exist, and when the absorption cross section cannot be equated to measured photoneutron cross sections. This situation sometimes arises for light nuclei. This method involves using a nuclear model calculation to estimate the ratio of (γ, xn) to (γ, abs) cross sections; and inferring the total absorption cross section (γ, abs) such that the calculated (γ, xn) agrees with measurements. This procedure has been described in model detail in Refs. [17,13].

II.B. Preequilibrium Emission

Preequilibrium reaction mechanisms become important for incident photon energies above 10-15 MeV. In the photoabsorption mechanisms described in the previous subsection, the initial nuclear excitation can be understood in terms of particle-hole excitations ($1p1h$ for the GDR; $2p2h$ or $2p1h$, as discussed later, for QD processes) and thus it is natural to use a preequilibrium theory of particle-hole excitations to describe the processes of preequilibrium emission, and damping to equilibrium, during the evolution of the reaction. Such models can be used to calculate photonuclear reactions for incident photons with energies up to about 150 MeV, which is just above the threshold for pion production.

Semiclassical preequilibrium models, such as the exciton and hybrid models, have proved

to be powerful tools for predicting particle emission spectra with a high degree of reliability, and in a computationally-fast manner [19,20,16,18]. Semiclassical models make use of detailed balance, and phase space considerations, to calculate emission rate probabilities from particle-hole states. By working in terms of emission rates, and not quantum mechanical transition amplitudes, some information is lost, particularly concerning observables sensitive to interference effects such as angular distributions and analyzing powers. Additionally, such models typically do not account for correlations in the particle-hole excitations. However, these deficiencies are to some extent compensated by the ease of implementation and high predictive power of the semiclassical theories. Semiclassical Intranuclear Cascade (INC) photonuclear models have also been developed [11,13,14]. These models have much in common with preequilibrium models. They differ, though, by following the trajectories of the excited nucleons in coordinate and momentum space (semiclassical preequilibrium models usually just follow the excitations in energy space), and by assuming that free nucleon-nucleon scattering cross sections can be used for in-medium nucleon scatterings. In practice, it is only the semiclassical preequilibrium models that have been implemented for photonuclear reactions, and the quantum multistep preequilibrium models [21] have not yet been extended for calculating these processes.

Two works in particular have demonstrated the usefulness of semiclassical preequilibrium models in describing photonuclear reactions: Wu and Chang's paper [19] on an exciton model; and Blann's studies [20] using the hybrid model; both of which utilize a Weisskopf-Ewing evaporation theory to describe the subsequent equilibrium decay. Wu and Chang used an initial $2p2h$ state in the preequilibrium cascade, while Blann argued that the two holes are correlated through the QD mechanism, and therefore can be approximated as one degree of freedom, i.e. a $2p1h$ initial state. Also, calculations by Ryckbosch *et al.* [22] indicated a preference for an initial $2p1h$ state when analyzing emission spectrum data at 60 MeV.

For the present work, the GNASH code has been developed to include a preequilibrium cascade following the excitation of particle-hole states in photoabsorption, using a master-

equation exciton model with an initial $2p1h$ state. Additionally, multiple-preequilibrium emission processes, where more than one fast preequilibrium ejectile is emitted in the reaction, are included using the theory of Ref. [23]. For both primary and multiple preequilibrium emission, the neutron-proton distinguishability factors were modified to reflect the initial particle-hole type appropriate for the QD mechanism (*i.e.* of the two particles, one is a neutron and the other a proton).

II.C. Compound Nucleus Equilibrium Emission

Following the possible emission of preequilibrium particles, the remaining nuclear system reaches equilibrium, after which it decays by sequential particle or gamma-ray emission until the residual nucleus ground state is reached.

Generally, the calculation of these equilibrium decay processes do not present any particular theoretical difficulties. The Hauser-Feshbach theory is applied, which includes angular momentum and parity conservation, and accounts for the fact that an E1-photon brings in one unit of angular momentum. The principal uncertainty entering these calculations is in the input information needed to compute equilibrium decay rates: nuclear level densities, optical model transmission coefficients and inverse reaction cross sections, and gamma-ray strength functions. The IAEA Reference Input Parameter Library (RIPL) [24] provides extensive guidance on the choice of these quantities. Additionally, we have been able to use many of the input parameter sets developed for our analyses of neutron and proton induced reactions on these same targets for the LA150 library [25].

II.D. Angular Distributions

A knowledge of the angular distribution of the ejectiles in photonuclear reactions is essential for radiation transport studies, but the GNASH code in its basic form yields only angle-integrated results. In nucleon-induced reactions, the Kalbach systematics [26] have been widely used for obtaining double-differential emission spectra. They are particularly

attractive for use in evaluation work since for each emission energy one need only specify the preequilibrium fraction (f_{MSD}) for the angular distribution to be defined, allowing a compact representation of angle-energy correlated cross sections. However, as originally formulated they cannot be applied in photonuclear reactions. Ideally, for applications it would be useful to parameterize measured angular distributions in monochromatic photon-induced reactions in the quasi-deuteron and giant dipole resonance (GDR) regimes, but an extensive experimental data set does not yet exist (larger amounts of experimental information exist for incident photons with a bremsstrahlung spectrum, but these data are not directly usable).

Below we summarize an applications-oriented method [27] for determining continuum photonuclear angular distributions for emission of light particles (n, p, d, t, ^{3}He, and α) for energies up to 150 MeV. Based on theoretical considerations by Chadwick and Oblozinsky [23] for the angular forward-peaking in preequilibrium reactions, Kalbach's 1988 angular distribution systematics [26] for a neutron projectile are modified for use in photon-induced reactions. This results in photonuclear angular distributions which are less forward-peaked than their nucleon-induced counterparts in the quasideuteron regime, due to the small momentum carried by a photon. In the GDR regime, a simple approximation of isotropy is assumed.

II.D.1 Giant-Dipole Region

At present, no general prescription is available for nuclear data evaluators for describing the angular distribution of secondary particles emitted in photonuclear reactions in the GDR regime. Experimental angular distributions for emitted nucleons from such collective excitations often show a dipole shape (peaking at 90-degrees), but nuclear structure effects are important in determining the detailed angular distribution and it is not clear that accurate systematics can be developed to describe them.

One of the main problems is that most measurements are for an incident bremsstrahlung spectrum, and not for monoenergetic photons. This is a problem because angular distributions are incident-energy dependent, and are also angle-energy correlated (*i.e.*, the angular

distribution varies for different secondary emission energies). Given this situation, two options appear available for evaluators:

1. Include angular distribution information based on available measured data

2. Assume isotropy in the GDR regime, for simplicity

The evaluations described in this paper follow the latter approach, except for carbon and oxygen where information from measurements is available and is used. It is hoped that for most applications, this is a reasonable starting point, and hopefully future work will result in a more accurate angular distribution representation within ENDF files.

II.D.2 Quasideuteron Region

Chadwick *et al.* [27] presented an approach for calculating the angular distribution of secondary ejectiles emitted in photonuclear reactions in the quasideuteron regime. The approach made use of the theoretical basis for the forward-peaking parameter "a" in the Kalbach systematics (originally developed for nucleons) [16,28], which was found to be dependent upon the momentum of the projectile. The low momentum of photons, compared to nucleons of the same energy, results in angular distributions which are much less forward-peaked than their nucleon counterparts.

This approach, which is presented below, allows evaluators to make use of the Kalbach systematics developed for nucleon projectiles, with a straightforward modification to the "a"-parameter.

II.D.3 Recommenced Systematics for Use in Evaluations

We recommend the applications-oriented method (Ref. [27]) to calculate continuum angular distributions of light particles (n, p, d, t, ^{3}He, and α) produced in photonuclear reactions based on Kalbach's 1988 systematics and the theoretical considerations given in Ref. [28]. The procedure for obtaining photonuclear angular distributions for a photon of energy $\leq$ 150 MeV in (γ, y) reactions, where y may represent all light ejectiles with mass $\leq$4, is:

- Determine the a^{ν} parameter for (n, y) reactions, for an incident neutron with energy E_{inc} from Kalbach's 1988 systematics.

- Obtain the photon-projectile a using:

$$a = a^{\nu}[\sqrt{E_{inc}/2m}]\ [min(4, max(1, 9.3/\sqrt{E_{em}}))], \tag{6}$$

where the a^{ν} parameter is taken from Kalbach's 1988 paper [26] for an incident neutron of the same energy as the photon projectile. The first modification factor to a^{ν} accounts for the lower photon momentum compared to a neutron, while the second factor approximately accounts for differences in refraction effects, and an upper limit of 4 for this correction to prevent it becoming unphysically large at low emission energies [27].

- Apply this a value in the following formulae:

$$\frac{d^2\sigma}{d\epsilon d\Omega} = \frac{d\sigma}{d\epsilon}\left[(1 - f_{MSD}(\epsilon))\frac{1}{4\pi} + f_{MSD}(\epsilon)g(\theta)\right], \tag{7}$$

where $f_{MSD}(\epsilon)$ is the fraction of the emission spectrum at emission energy ϵ coming from preequilibrium processes. An isotropic distribution for the non-precompound contribution is assumed. The quasideuteron angular distribution shape is given by:

$$g(\theta) = \frac{1}{4\pi}\frac{2a}{e^{a} - e^{-a}}\exp(a\cos\theta). \tag{8}$$

In the present work, the above angular distribution systematics are used as a sampling distribution function in the MCNP and MCNPX Monte Carlo transport code (see Ref. [4] for more details). An attractive feature of the angular distribution Eq. (8) is that it can be integrated analytically, so that angles can be sampled in a Monte Carlo approach using a closed-form expression. The probability of a particle being scattered to an angle θ is proportional to $g(\theta)\sin(\theta)$. To sample from this distribution, it must be integrated from θ=0 to θ' - the sampled value for θ corresponds to the value of θ' for which the integral

equals a random number R chosen between zero and unity. This then gives a sampled theta as:

$$\theta' = \arccos\left[\ln[\exp(a) - R(\exp(a) - \exp(-a))]/a\right]. \tag{9}$$

Therefore, to Monte Carlo sample the angular distribution Eq. (7), two random numbers must be chosen: (1) to determine whether an isotropic distribution (the first term in Eq. (7)) or a forward-peaked distribution (the second term in Eq. (7)) is to be used, dependent on whether or not the random number is below the value of $f_{MSD}(\epsilon)$; (2) to sample an isotropic distribution, or a forward-peaked distribution using Eq. (9).

II.E. Illustrative Comparisons with Experiment

A difficulty in testing photonuclear reaction theories that model nucleon emission spectra is the lack of experimental data to compare the model predictions against. While photoneutron and photoproton emission spectra from bremsstrahlung photon sources are not uncommon, such measured spectra from monoenergetic ("monochromatic") photon incident beams are sparse. A few monoenergetic photon-induced experiments do exist though [29,22], and in addition, quasi-monoenergetic photon-induced spectra have been inferred using the difference-technique, where two bremsstrahlung-induced emission spectra, with different end-points, are subtracted to approximate the spectrum due to a monoenergetic source. These measurements are described in more detail below.

One way to circumvent problems in validating emission spectra calculations given the lack of differential monoenergetic photon-induced measurements, is to test the theoretical predictions of partial exclusive reaction channels (e.g. $(\gamma, 1n), (\gamma, 2n)$, etc), along with neutron emission multiplicities, against experimental measurement. These measurements indirectly test the calculated emission spectra. This is because the energy-dependence of the calculated photon emission spectra strongly influences the exclusive reaction channels populated, by energy balance. An example is shown in Fig. 1, for photons incident on

^{208}Pb. The GNASH calculation is seen to describe the partition of the absorption cross section amongst the $(\gamma, 1n)$, $(\gamma, 2n)$, $(\gamma, 3n)$ channels well. This particular example illustrates another difficulty that one faces when analyzing experimental measurements – discrepancies between data measured at different laboratories. In this case we have adopted Berman's view [30] that the data from Saclay should be renormalized down by 7 % and that the older data from Livermore should be renormalized up by 22%.

As an illustrative example of the use of neutron emission multiplicities to test the model calculations, Fig. 2 shows calculated average multiplicities for neutron emission compared with the measurements of Lepretre *et al.* [31]. There is a nice discussion in Lepretre's paper [31] commenting on the slope of the average neutron multiplicity curve, which is worth repeating: If preequilibrium emission did not occur, each emitted neutron would require approximately 10 MeV (separation energy plus evaporation kinetic energy), and so the multiplicity curve would increase at a slope of 1 unit for every 10 MeV incident energy. The data in Fig. 2 show such a steep slope at the lowest incident energies, but for higher energies a much smaller slope occurs due to the higher kinetic energy carried by preequilibrium ejectiles. These data, therefore serve to indirectly validate that calculated emission spectra.

Figure 3 shows measured fast and slow multiplicities at an incident photon energy of 70 MeV [31], compared with calculations (shown for all energies up to 150 MeV). The fast multiplicity refers to the preequilibrium particles, while the slow multiplicity refers to the compound nucleus particles, and the calculations are seen to describe the correct partitioning of ejectiles among preequilibrium and equilibrium emission, and between neutrons and protons. These measurements are invaluable for testing the preequilibrium modeling in the calculation, since direct measurements of the nucleon emission spectra from monoenergetic photons do not exist for lead. The large Coulomb barrier in lead is responsible for the excess of fast preequilibrium neutrons compared to protons; at the highest energies the differences are reduced. In general the slow neutron multiplicity is much larger than the fast multiplicities, since preequilibrium decay accounts for at most the first two emissions, with the subsequent sequential particle decays coming from compound-nucleus emission.

Figure 4 shows an example of calculated 60 MeV proton emission spectra at 90-degrees compared with data [22], for the $^{40}Ca(\gamma, xp)$ reaction at 60 MeV. The angular variation was obtained using the approach described above and in Refs. [16,27]. The calculated photoproton emission spectrum describes the measurements well. This is important because there are very few sets of measured emission spectra data for monoenergetic incident photons to test the theory. Other tests of the calculated emission spectra were presented in Ref. [27], using the carbon experimental data of McGeorge *et al.* [29].

III. ENDF FORMATS AND NJOY DATA PROCESSING

The evaluations provides a complete representation of the nuclear data needed for transport, damage, heating, radioactivity, and shielding applications over the incident photon energy range from threshold up to 150 MeV. The evaluation utilizes "MT=5" to represent all reaction data. For readers who are not ENDF afficionados, this means that inclusive production cross sections are represented, rather than individual exclusive reaction channels. This approach is considered adequate for most applications, and was adopted because it becomes impractical to represent each of the many exclusive channel cross sections for higher incident energies. Furthermore, this procedure was used in our work on neutron and proton evaluations up to 150 MeV [25], and is recommended by Koning's Nuclear Energy Agency subgroup [32].

Production cross sections and emission spectra are given for neutrons, protons, deuterons, tritons, alpha particles, gamma rays, and all residual nuclides produced (A¿5) in the reaction chains. To summarize, the ENDF sections used are:

file-3, MT=5 Photoabsorption (total nonelastic) cross section

file-3, MT=5 Multiplicities (yields) for production cross sections, and energy-angle distributions for emission neutrons, protons, deuterons, tritons, alphas; and angle-integrated spectra for gamma rays and residual nuclei that are stable against particle emission.

The angle-energy correlated emission spectra for the light (A$\leq$4) ejectiles make use of the approach described above in Sec. II.D.3., *i.e.* an energy-spectrum is tabulated together with a preequilibrium fraction f_{MSD} for each emission energy. This compact representation allows the angular distribution to be sampled in the Monte Carlo code, the a parameter having been provided by the NJOY code (see below).

The exclusive cross sections for $(\gamma, 1n)$, $(\gamma, 2n)$, $(\gamma, 3n)$, $(\gamma, 1p)$, $(\gamma, 2p)$, *etc.*, are not given explicitly as reactions with MT = 4, 16, 17, 103, 111, respectively. These cross sections are readily available, however, from the multiplicities tabulated for the various residual nuclei corresponding to the above reactions. Such cross sections are very useful for comparing with experimental data, such as is given in the compilation by Dietrich and Berman [6].

The above approach was used for all our evaluations except carbon and oxygen. Because direct neutron and proton emission processes that leave the residual nucleus in its ground state are particularly important in these nuclei, the $(\gamma, n0)$ and $(\gamma, p0)$ channels were explicitly represented using MT=50, and MT=600, respectively, and angular distributions were provided using Legendre polynomials. The cross section after these direct reactions have been accounted for was represented using MT=5 as described above.

IV. RESULTS

In this section our results our presented for photonuclear reaction evaluated data for reactions on Pb, W, Ta, Cu, Fe, Ca, Si, Al, O, and C. The descriptions for each target nucleus includes a summary of the assumptions made during the evaluation procedure. Because of space limitations, for the most part we only compare the calculated results with experimental data for the absorption cross section (γ, abs) and the total neutron production cross section (γ, xn).

For photonuclear reactions on the lead isotopes, there are systematical differences between some of the important measurements of neutron production. Specifically, the results from Saclay are significantly higher than those from Livermore. Berman [30] concluded that the earlier Livermore measurements on lead [33] were too low. We have adopted Berman's view that the Saclay data [34] need to be renormalized down by 7%, and the Livermore data [33] for lead need to be renormalized up by 22%. The absorption cross section calculated from a Lorentzian form in the GDR regime was modified on the low-energy tail where deviations from experimental data are seen. Above the GDR, in the QD regime, we then evaluated the absorption x/s up to 150 MeV based on experimental data [35] and model calculations [15]. The resulting absorption cross section for ^{208}Pb is shown in Fig. 5 compared with measurements.

GNASH model calculations were subsequently used to compute the individual channel cross sections, the total secondary particle production cross sections, and the secondary ejectile spectra. Illustrative figures showing the individual $(\gamma, 1n)$, $(\gamma, 2n)$, $(\gamma, 3n)$, *etc* cross sections were given in Section II.E. Our evaluations for neutron production for ^{206,7,8}Pb are in good agreement with (renormalized) data [33,34,36,35], see Fig. 6

A. IV.B. Tungsten

For tungsten we have produced an evaluation just for the major isotope, ^{184}W. However, our evaluation can be adopted for a representation of elemental tungsten since it is in good agreement with elemental measured data. The calculated photoabsorption cross section was based upon GDR Lorentzian and QD parameters chosen to agree with the elemental tungsten photoabsorption cross section from Saclay [37]. This also resulted in good agreement with the measurements of Gurevich [38]. At the higher energies, use was made of the total tantalum absorption cross section data of Lepretre *et al.* [35] to guide the quasideuteron

model calculation of the absorption cross section, giving a Levinger parameter of L=6.7. (No such data exists for W, but we expect W and Ta experimental data to be similar). The evaluated absorption cross section is shown in the upper graph of Fig. 7 for incident energies up to 150 MeV. Good agreement was obtained for (γ,1n) and (γ,2n) calculated with GNASH compared to the elemental tungsten experimental data from Saclay [37]. Our calculation of the total photoneutron production compared with the elemental data from Saclay is shown in the lower graph of Fig. 7.

B. IV.C. Tantalum

Photonuclear reactions on tantalum have been studied recently by Lee, Fukahori, and Chang [18]. Lee *et al.* [18] noted that the Saclay data [39] and the Livermore [40] data are discrepant, and that the discrepancy has been studied by the Sao Paulo group [41,42]. They concluded that the Livermore multiplicity is correct, while the Saclay sorting erroneously interpreted (γ,2n) events as two (γ,1n) events. However, the magnitude of the Livermore data is too low, by a factor of 1.22. Using these arguments, Lee derived newly reanalyzed "experimental" data – the Saclay (γ,1n) and (γ,2n) data are modified, as is the (γ,abs) data, but the (γ,3n) and (γ,xn) Saclay data remain unchanged. Lee's paper fits GDR parameters to the newly constructed photoabsorption data, and uses the quasideuteron absorption model [15] with a Levinger parameter of L=6.5, which fits Lepretre's data well [35,15].

In the present evaluation, we make use of the reanalyzed Saclay measurements of Lee [18], and use their values for the photoabsorption GDR and QD parameters. The measured $(\gamma, 1n)$, $(\gamma, 2n)$, $(\gamma, 3n)$, (γ, xn) data are used to validate the GNASH calculations, which are found to describe these data well. The absorption cross section and the total neutron production cross section are shown in Fig. 8, compared with the Saclay data as reanalyzed by Lee *et al.*. Data of Lepretre [31], for the total emitted neutron multiplicity, were used to test the model calculations, for incident energies up to 150 MeV (Fig. 9).

C. IV.D. Copper

Our evaluation is for the major copper isotope, ^{63}Cu. No data exist for the total absorption cross section. However, data do exist for the photoneutron cross section [43], and the GNASH code predicts the ratio of (γ, abs) to (γ, n) and (γ, p). Thus, we relied on the GNASH code to infer the absorption cross section in the GDR regime, so as to model accurately the Fultz (γ, xn) measured data [43]. However, based on previous studies that have concluded that the Livermore data are systematically too low, we have renormalized up the Livermore Fultz data by a factor 1.17 below 35 MeV. This led to agreement with Varlamov's photoneutron data [44,45] at the peak of the Giant Resonance. The total absorption cross section above the GDR, up to 150 MeV, was taken from quasideuteron model calculations [15].

The $(\gamma, 1n + np)$ calculated data were in fairly good agreement with those of Fultz x 1.17 [43], Varlamov [44,45], and Martins [46], though were on the high side of the measurements near 23 MeV. Likewise, the $(\gamma, 2n)$ calculated data were low at 23 MeV compared to the Fultz x 1.17 measurements, but these two defects compensated each other and the (γ, xn) calculated results agreed with the data, see Fig. 10.

D. IV.E. Iron

Very little measured photonuclear data exist for ^{56}Fe, or even natural iron. Thus, spherical Lorentzian parameters for the GDR were taken from Kishida's systematics [17], based on the work of Berman, Carlos, and others. This gave E=18.2 MeV, Γ=6.6 MeV. The GDR peak cross section was evaluated to be 89. mb so that the GNASH calculated $(\gamma, 1n)$ cross section at 17.5 MeV gave 63 mb in agreement with data of Costa [47], as tabulated in Varlamov's Photonuclear Data Index [48]. Furthermore, the absorption peak of 89 mb is in good agreement with the measurement of Dolbilkin [49] who obtained 90 mb, see Ref. [48]. To the GDR absorption component was added a quasideuteron component from model calculations,

with a Levinger parameter of 6.5 taken from theory [15]. Figure 11 shows the evaluated absorption and single photoneutron cross sections compared with these measurements. The sharp rise in the photoneutron cross section seen at 11.2 MeV in Fig. 11 corresponds to that channel's threshold; at lower energies photoabsorption leads to the emission of protons and alpha particles.

E. IV.F. Calcium

The photoabsorption cross section was evaluated based on the data of Ahrens [50], that extend up to 150 MeV. At 60 MeV, the value for the absorption cross section was consistent with that used by Ryckbosch *et al.* [22]. Measurements [22] of the inclusive photoproton spectra for 62 MeV Ca(γ,xp) at 90-degrees were shown in Fig. 4.

The total photoabsorption cross section is used as an input into the GNASH calculations. These calculations then predict the branching to photoneutron, photoproton, *etc.* emission. The calculated photoneutron production was compared with measurements of Veyssiere [51]. The calculations, after a level density adjustment for ^{39}Ca, predicted the (γ,xn) data of Veyssiere [51] reasonably well, with the exception of the 25-30 MeV region where the calculated photoneutron production appears to be about 20% too high (Fig. 12. This illustrates a weakness in the model calculation capability, where adjustment of input level density parameters within reasonable physical ranges still did not yield consistency with the measured data above 25 MeV.

F. IV.G. Silicon

The analysis of photonuclear reactions on light nuclei using a Hauser-Feshbach code can pose some problems because of the role of isospin conservation. For light nuclei, where the Coulomb interactions are relatively small, the isospin quantum number is expected to be conserved at a relatively high level in nuclear reactions. In the case of isospin $T = 0$ targets, such as ^{28}Si as well as ^{16}O and ^{12}C discussed below, this has the consequence that

alpha particle emission should be strongly suppressed for low photon energies because of isospin conservation. This is because the photon projectile has $T = 1$, the emitted alpha particle has $T = 0$, and therefore $T = 0$ states in the final nucleus after alpha emission cannot be populated. For targets of ^{28}Si, ^{16}O, and ^{12}C, the corresponding residual nuclei after alpha emission are ^{24}Mg, ^{12}C, and ^{8}Be respectively, and these nuclei have $T = 0$ states at low excitation energies, and only have $T = 1$ states that can be populated via isospin conservation at higher energies.

Because of these considerations, it is to be expected that a Hauser-Feshbach code such as GNASH, that does not include isospin conservation, would largely overpredict alpha emission for photon energies just above the alpha emission threshold. In our analyses of ^{28}Si, ^{16}O, and ^{12}C, this indeed was the case. We solved the difficulty in an ad-hoc manner by artificially suppressing alpha particle emission in our GNASH calculations, so as to adequately predict the measured magnitude of the main competition decay processes, *i.e.* neutron and proton emission. We note that no general purpose Hauser-Feshbach code that includes isospin conservation is available, to our knowledge, though we have studied ad-hoc modifications to the GNASH code to include the necessary Clebsch-Gordan isospin coupling coefficients [52].

In our evaluation of silicon the photoabsorption cross section was based on the elemental data of Ahrens [50] that extends up to 30 MeV, with a result that closely follows the evaluation by Lee *et al.* described in Ref. [9]. The GNASH model calculations predicted secondary neutron emission that was in good agreement with measurements [51,53–55] of $1n + np$ neutron emission, as shown in Fig. 13.

G. IV.H. Aluminum

The photoabsorption cross section was evaluated based on the data of Ahrens [50], that extend up to 150 MeV. However, above about 35 MeV, the evaluation used directly theoretical predictions from the quasideuteron model [15]. Between approx. 30-40 MeV, the evaluation underpredicted the Ahrens absorption data. This was done since the evaluated

neutron production in this energy range, based on GNASH predictions, somewhat over-predicted the photoneutron production measurements (see below), and it was felt that it is important to have as accurate as possible predictions of photoneutron production; increasing the absorption cross section here would lead to a worse discrepancy with the photoneutron production data.

The GNASH calculations gave an accurate representation of measured data at the GDR peak (21 MeV): a neutron production of about 15mb in agreement with Refs. [56,51]; a proton production about 16 mb (experiment = 17.5 mb [48]); and an alpha production of 11 mb, with the sum adding up to 41 mb as predicted by Ahrens [50]). Our default calculations used the A=20-40 level density systematics of Grimes, and gave reasonably good agreement with measurements at the GDR peak, but the parameters were subsequently modified, through changing the pairing and shell shifts, so better account for the data. After this, the same set of parameters were used for all incident energies.

The calculated results were compared with measurements from Refs. [56,51] of 1n and 2n neutron emission (or more precisely, 1n+1np cross sections, and 2n+2np cross sections, since the charged-particle channels are not small). The 2n+2np channel was on the high-side of the measurements, and we were unable to obtain lower calculated values without using physically-unreasonable level density parameters. In consequence, the calculated (γ,xn) neutron production cross section was in good agreement with experiment [56,51] up to 30 MeV, but was on the high-side of the data from 30-37 MeV, where the 2n+2np channels contribute. The absorption and the photoneutron cross sections are shown in Fig. 14.

H. IV.I. Oxygen and Carbon

We describe our results for carbon and oxygen in the same subsection because we adopted the same evaluation procedure for these nuclei, which differs in certain respects from our previous evaluations for heavier nuclei. Our evaluations for carbon and oxygen are dependent to a greater extent on measured data compared to our evaluations for heavier target nuclei,

which were mainly dependent upon nuclear statistical model calculations. One of the reasons for this is the importance of direct reactions in which high energy neutrons and protons are emitted, leaving the residual nucleus in its ground state [$(\gamma, n0)$ and $(\gamma, p0)$ reactions]. Furthermore, the statistical model is less reliable for compound nucleus calculations in light nuclei (and see discussion in Sec. IV.G that addresses isospin considerations).

For oxygen, our evaluation of photonuclear reactions follows, to a large extent, the comprehensive analysis described by Fuller [57]. The photoabsorption cross section was evaluated based on the data of Ahrens [50], that extend up to 150 MeV. Below 30 MeV, a constant value of 2.78 mb was subtracted from these data, as recommended by Fuller, in order to make these data consistent with the sum of other (γ, n), (γ, p), *etc.* data. However, no such subtraction was made for energies above 50 MeV since this would result in negative cross sections, and a smooth transition was used for the absorption cross section from 30 to 50 MeV, see Fig. 15, upper graph.

The $(\gamma, n0)$ and $(\gamma, p0)$ processes, which result in the residual nucleus being left in its ground state, account for a significant fraction of the photonuclear cross section (particularly for incident energies below 30 MeV). Therefore we first evaluate the ^{16}O $(\gamma, n0)$ and $(\gamma, p0)$ cross sections from the available experimental data. We adopt Fuller's recommendations [57] for these data (Fig. 15, upper graph), together with extensions to higher energies based upon Phillips' results [58]. In the case of the $(\gamma, p0)$ data, these are based on the inverse process of proton capture. For the $(\gamma, n0)$ and $(\gamma, p0)$ we also provide angular distributions in the ENDF file using Legendre polynomials. These were obtained from Phillips' paper [58], for both $(\gamma, n0)$ and $(\gamma, p0)$ [1]

The remaining cross section after $(\gamma, n0)$ and $(\gamma, p0)$ processes have occurred is modeled with the GNASH code, and represented in the ENDF file using MT5, that is, as inclusive

---

[1]Note that Phillips' text describing the $(\gamma, p0)$ Legendre is not consistent with the data in his figure 7; Phillips advised us to use the graphical data rather than that based on the text.

production data. Preequilibrium and compound decay processes are included. The resulting neutron emission contribution, when added to the $(\gamma, n0)$ cross section, was compared (Fig. 15, lower graph) with Fuller's evaluation, and other measurements [51,59,60], and good agreement was obtained.

For carbon, our evaluation also follows, to a large extent, the analysis described by Fuller [57]. The photoabsorption cross section was evaluated based on the data of Ahrens [50], that extend up to 150 MeV. Below 30 MeV, a constant value of 0.7 mb was subtracted from these data, as recommended by Fuller, see Fig. 16.

As was the case for oxygen, the carbon $(\gamma, n0)$ and $(\gamma, p0)$ reactions, which result in the residual nucleus being left in its ground state, account for a significant fraction of the photonuclear cross section below 30 MeV. Therefore again we first evaluate these cross sections from the available experimental data (Fig. 17). We adopt Fuller's recommendations [57] in the GDR region; at higher energies our evaluation is based on the Matthews [61] data at 60, 80, and 100 MeV for $(\gamma, p0)$ reactions, and we assume an equal cross section for the $(\gamma, n0)$ reactions at these high energies motivated by the concept of quasideuteron reaction mechanism. We adopted dipole angular distribution shapes (the only non-zero Legendre coefficient being $a2$) taken from Ref. [57].

The remaining cross section after $(\gamma, n0)$ and $(\gamma, p0)$ have occurred is modeled with the GNASH code, and represented in the ENDF file using MT5 as inclusive production data. Preequilibrium and compound decay processes are included. The resulting neutron emission contribution, when added to the $(\gamma$,n0) cross section, was compared with Fuller's evaluation based on a renormalization of Fultz's data [56] by a factor 1.17. Reasonable agreement for neutron production was obtained in the GDR peak (Fig. 16), though the calculations overpredict neutron production (by as much as 30%) by 30 MeV. This failing is due to the difficulties in using a Hauser-Feshbach code to model reactions on light nuclei. Finally, we note that GNASH calculations [16] of proton emission spectra for 60 MeV incident photons agreed well with the double differential data of McGeorge [29].

V. CONCLUSIONS

We have described model calculations and evaluated data files for photonuclear reactions on a number of materials important in accelerator technologies. These evaluations, which we refer to collectively as the "LA150.G" library, will be submitted for inclusion in the ENDF/B-VI library available from the National Nuclear Data Center at Brookhaven [1]. They are currently available over the internet at http://t2.lanl.gov/data/he.html, together with plots of the data that include 2-D plots of cross sections and 3-D perspective plots of the energy distributions for emitted particles and photons. We reiterate that a suite of over 160 photonuclear evaluations, including those described here, will shortly be released by the International Atomic Energy Agency [9].

These data facilitate quantitative radiation transport calculations of the importance of photonuclear reactions in a number of applications, including photoneutrons produced in electron/photon accelerators, shielding studies, and nondestructive detection of nuclear materials. The next back-to-back paper describes developments to the MCNP and MCNPX codes to utilize these photonuclear data in fully-coupled transport simulations [4].

VI. ACKNOWLEDGMENTS

We gratefully acknowledge useful discussions with Dr. Laurie Waters, of the APT Technical Project Office at Los Alamos, who supported the bulk of the work described here. We have had useful discussions with Drs. M. Blann, T. Brown, T. Phillips, S. Frankle, R. Haight, G. Hughes, R. Prael, and we are particularly grateful for useful discussions and collaborations with members of the IAEA photonuclear project: Drs. P. Oblozinsky, A. Blokhin, Y. Boasheng, T. Fukahori, Y.O. Lee, M. Martins, V. Varlamov, and J. Zhang.

REFERENCES

[1] C. L. DUNFORD, Internet connection to the National Nuclear Data Center (NNDC), 1998, Brookhaven National Laboratory: WWW address: http://www.nndc.bnl.gov/.

[2] F. X. GALLMEIER, "Photoneutron production in MCNP4A," in *Proc. of ANS Topical Meeting on Radiation Protection and Shielding*, pp. 780–786, R. J. Cacciapouti, Ed., American Nuclear Society La Grange Park, IL, No. Falmouth, Massachusetts, April 21-25 (1996).

[3] M. B. CHADWICK, T. H. BROWN, AND R. C. LITTLE, "Photoneutron production in electron beam stop for Dual Axis Radiographic Hydrotest Facility (DARHT)," in *Proceedings of the 1998 Radiation Protection and Shielding Division Topical Conference*, Los Alamos Report LA-UR-97-5174, Nashville, Tennessee, April 19-23, 1998 pp. Vol. 2, 356–363, American Nuclear Society, La Grange Park, IL (1998).

[4] M. C. WHITE *et al.*, *Nucl. Sci. Eng.* (2000, submitted).

[5] M. C. WHITE, R. C. LITTLE, AND M. B. CHADWICK, "Photonuclear physics in MCNP(X)," in *Proceedings of the ANS on Nuclear Applications of Accelerator Technology*, Long Beach, California, November 14-18, 1999, pp. 515–519, VanTuyle, G., Ed., American Nuclear Society, La Grange Park, IL (1999).

[6] S. S. DIETRICH AND B. L. BERMAN, *Atomic Data and Nuclear Data Tables* **38**, 199 (1988).

[7] A. V. VARLAMOV, V. V. VARLAMOV, D. S. RUDENKO, AND M. E. STEPANOV, "Atlas of Giant Dipole Resonance Paramaters and Graphs of Photonuclear Reaction Cross Sections," INDC (NDS)-394, International Atomic Energy Agency, (1999).

[8] IAEA, "Compilation and Evaluation of Photonuclear Data for Applications," in *Summary Report of IAEA 1-st Research Coordination Meeting*, No. INDC(NDS)-364, P. Oblozinský, Ed., International Atomic Energy Agency, Vienna, Austria, Obninsk, Rus-

sian Federation, December 7-10, 1996 (1997).

[9] P. OBLOZINSKY *et al.*, "Handbook of photonuclear data for applications," IAEA-TECDOC, International Atomic Energy Agency, (2000, in press).

[10] R. G. ALSMILLER, T. A. GABRIEL, AND M. P. GUTHRIE, *Nucl. Sci. Eng.* **40**, 365 (1970).

[11] T. A. GABRIEL, *Phys. Rev. C* **13**, 240 (1976).

[12] A. FASSO, A. FERRARI, AND P. R. SALA, "Designing electron accelerator shielding with FLUKA," in *Proc. of 8th. International Conference on Radiation Shielding*, Arlington, Texas, April 24-28, 1994 pp. 643–649, American Nuclear Society, La Grange Park, IL (1994).

[13] A. FASSO, A. FERRARI, AND P. R. SALA, "Total Giant Resonance Photonuclear Cross Sections for Light-Nuclei: A Database for the FLUKA Monte Carlo Transport Code," in *Proc. of Third Specialists Meeting on Shielding Aspects of Accelerators, Targets, and Irradiation Facilities (SATIF-3)*, Tohoku University, Sendai, Japan, 12-13 May 1997 pp. 61–74, Organization for Economic Cooperation and Development (OECD) Nuclear Energy Agency, Paris, France (1998).

[14] N. V. MOKHOV, S. I. STRIGANOV, A. VAN GINNEKEN, S. G. MASHNIK, A. J. SIERK, AND J. RANFT, "MARS Code Developments," in *Proc. of Fourth Specialists Meeting on Shielding Aspects of Accelerators, Targets, and Irradiation Facilities (SATIF-4) (LANL report LA-UR-5716 (1998))*, Knoxville, Tennessee, September 14-16 1998 Organization for Economic Cooperation and Development (OECD) Nuclear Energy Agency, Paris, France (1998).

[15] M. B. CHADWICK, P. OBLOZINSKY, P. E. HODGSON, AND G REFFO, *Phys. Rev. C* **44**, 814 (1991).

[16] M. B. CHADWICK AND P. G. YOUNG, *Acta Physica Slovakia* **45**, 633 (1995).

[17] N. KISHIDA, "Methods used in photonuclear data evaluation at JNDC," in *Proc. of the Symposium on Nuclear Data Evaluation Methodology*, Brookhaven National Laboratory, Upton, NY, 12-16 Oct. 1992, p. 598, C.L. Dunford, Ed., World Scientific, Singapore (1993).

[18] Y-O LEE, T. FUKAHORI, AND J CHANG, *Journal of Nuclear Science and Technology* **35**, 685 (1998).

[19] J. R. WU AND C. C. CHANG, *Phys. Rev. C* **16**, 1812 (1977).

[20] M. BLANN, B. L. BERMAN, AND T. T. KOMOTO, *Phys. Rev. C* **28**, 2286 (1983).

[21] H. FESHBACH, A. KERMAN, AND S. KOONIN, *Ann. Phys. (N.Y.)* **125**, 429 (1980).

[22] D. RYCKBOSCH, L. VANHOOREBEKE, R. VANDEVYVER, F. DESMET, J. O. ADLER, D. NILSSON, B. SCHRODER, AND R. ZORRO, *Phys. Rev. C* **42**, 444 (1990).

[23] M. B. CHADWICK, P. G. YOUNG, D. C. GEORGE, AND Y. WATANABE, *Phys. Rev. C* **50**, 996 (1994).

[24] *Handbook for Calculations of nuclear reaction data: Reference input parameter library* No. IAEA-TECDOC-1034, International Atomic Energy Agency, Vienna, Austria (1998, http://www-nds.iaea.or.at/ripl).

[25] M. B. CHADWICK, P. G. YOUNG, S. CHIBA, S. FRANKLE, G. M. HALE, H. G. HUGHES, A. J. KONING, R. C. LITTLE, R. E. MACFARLANE, R. E. PRAEL, AND L. S. WATERS, *Nucl. Sci. Eng.* **131**, 293 (1999).

[26] C. KALBACH, *Phys. Rev. C* **37**, 2350 (1988).

[27] M. B. CHADWICK, P. G. YOUNG, AND S. CHIBA, *Journal of Nuclear Science and Technology* **32**, 1154 (1995).

[28] M. B. CHADWICK AND P. OBLOZINSKY, *Phys. Rev. C* **50**, 2490 (1994).

[29] J. C. McGeorge and *et al.*, *Phys. Lett. B* **179**, 212 (1986).

[30] B. L. Berman, R. E. Pywell, S. S. Dietrich, M. N. Thompson, K. G. McNeill, and J. W. Jury, *Physical Review* **36**, 1286 (1987).

[31] A. Lepretre, H. Beil, R. Bergere, P. Carlos, J. Fagot, A. Veyssiere, and I. Halpern, *Nucl. Phys. A* **390**, 221 (1982).

[32] A. J. Koning, T. Fukahori, and A. Hasegawa, "Volume 13: Intermediate Energy Data," NEA/WPEC-13, Nuclear Energy Agency, (1998a).

[33] R. R. Harvey, *Phys. Rev.* **136**, B126 (1964).

[34] A. Veyssiere, H. Beil, R. Bergere, P. Carlos, and A. Lepretre, *Nucl. Phys.* **A159**, 561 (1970).

[35] A. Lepretre, H. Beil, R. Bergere, P. Carlos, J. Fagot, A. De Miniac, and A. Veyssiere, *Nucl. Phys. A* **367**, 237 (1981).

[36] L. M. Young, PhD. thesis, University of Illinois, 1972.

[37] A. Veyssiere, H. Beil, R. Bergere, P. Carlos, A. Lepretre, and A. Deminiac, *J. de Physique Lettres* **36**, L267 (1975).

[38] G. M.. Gurevich *et al.*, *Nucl. Phys. A* **351**, 257 (1981).

[39] R. Bergere, *Nucl. Phys.* **A121**, 463 (1968).

[40] R. L. Bramblett, *Phys. Rev.* **129**, 2723 (1963).

[41] E. Wolynec, A. R. V. Martinez, P. Gouffon, Y. Miyao, V. A. Serrao, and M. N. Martins, *Phys. Rev. C* **29**, 1137 (1984).

[42] M. N. Martins in, "Compilation and Evaluation of Photonuclear Data for Applications," in *Summary Report of IAEA 1-st Research Coordination Meeting*, No. INDC(NDS)-364, P. Oblozinský, Ed., International Atomic Energy Agency, Vi-

enna, Austria, Obninsk, Russian Federation, December 7-10, 1996 (1997).

[43] S. C. FULTZ, *Rev. Mod. Phys.* **133**, B1149 (1964).

[44] V. V. VARLAMOV, N. G. EFIMKIN, AND B. S. ISHKHANOV, "Simultaneous Analysis of Discrepant Photonuclear Data," in *Proc. of the International Conference on Nuclear Data for Science and Technology*, Gatlinburg, TN, 1994, p. 662, J.K. Dickens, Ed., American Nuclear Society, La Grange Park, IL (1994).

[45] V. V. VARLAMOV, N. G. EFIMKIN, B. S. ISHKHANOV, V. V. SAPUNENKO, AND M. STEPANOV, *Izvestiya Akademii Nauk Seriya Fizicheskaya* **59**, 223 (1995).

[46] M. N. MARTINS, E. HAYWARD, F. LAMAZE, X. K. MARUYAMA, F. G. SCHIMA, AND E. WOLYNEC, *Phys. Rev. C* **30**, 1855 (1984).

[47] S. COSTA, *Nuovo Cim.* **51B**, 199 (1967).

[48] V. V. VARLAMOV AND V. V. SAPUNENKO, "Photonuclear Data Index 1976 - 1995," Izdatel'stvo Moskovskogo Universiteta, Moscow State University, (1996).

[49] B. S. DOLBILKIN, *Yad. Fiz.* **9**, 675 (1969).

[50] J. AHRENS, *Nucl. Phys.* **A251**, 479 (1975).

[51] A. VEYSSIERE, *Nucl. Phys.* **A227**, 513 (1974).

[52] F. B. BATEMAN, R.C. HAIGHT, M. B. CHADWICK, S. M. STERBENZ, S. M. GRIMES, AND H. VONACH, *Phys. Rev. C* **60**, 064609 (1999).

[53] J. T. CALDWELL, R. R. HARVEY, R. L. BRAMBLETT, AND S. C. FULTZ, *Physics Letters* **6**, 213 (1963).

[54] B. I. GORYACHEV, B. S. ISHKHANOV, V. G. SHEVCHENKO, AND B. A. YURYEV, *Yad. Fiz.* **2**, 1168 (1968).

[55] R. E. PYWELL, B. L. BERMAN, J. W. JURY, J. G. WOODWORTH, K. G. MCNEILL,

AND N. T. THOMPSON, *Phys. Rev. C* **27**, 960 (1983).

[56] S. C. FULTZ, *Phys. Rev.* **143**, 790 (1966).

[57] E. G. FULLER, *Physics Reports* **127**, 187 (1985).

[58] T. W. PHILLIPS AND R. G. JOHNSON, *Physical Review* **C20**, 1689 (1979).

[59] B. L. BERMAN, J. W. JURY, J. G. WOODWORTH, R. E. PYWELL, K. G. MCNEILL, AND M. N. THOMPSON, *Physical Review* **C27**, 1 (1983).

[60] U. KNEISSL, G. KUHL, K. H. LEISTER, AND A. WELLER, *Nuclear Physics* **A127**, 1 (1975).

[61] J. L. MATTHEWS, *Nucl. Phys.* **A267**, 51 (1976).

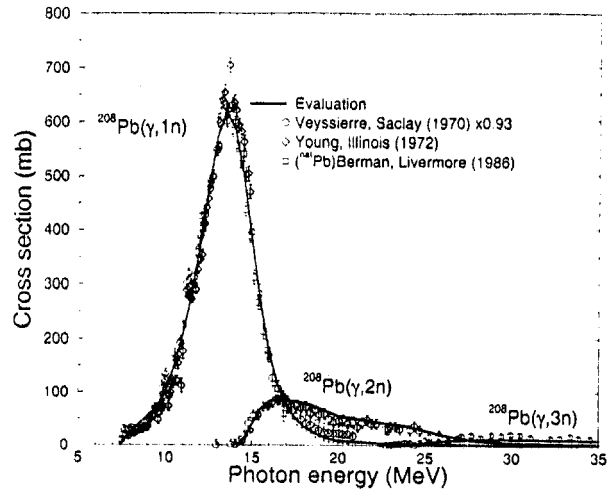

FIG. 1. Evaluated photoneutron cross sections, based on GNASH code calculations, for ^{208}Pb compared with measurements.

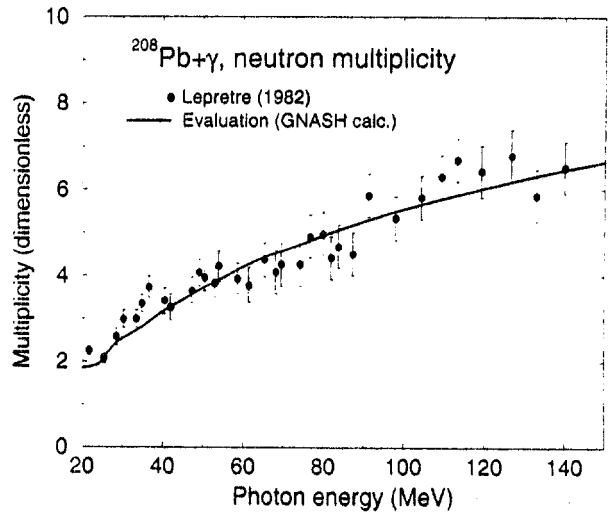

FIG. 2. Evaluated average photoneutron multiplicity, based on GNASH code calculations, for ^{208}Pb compared with measurements.

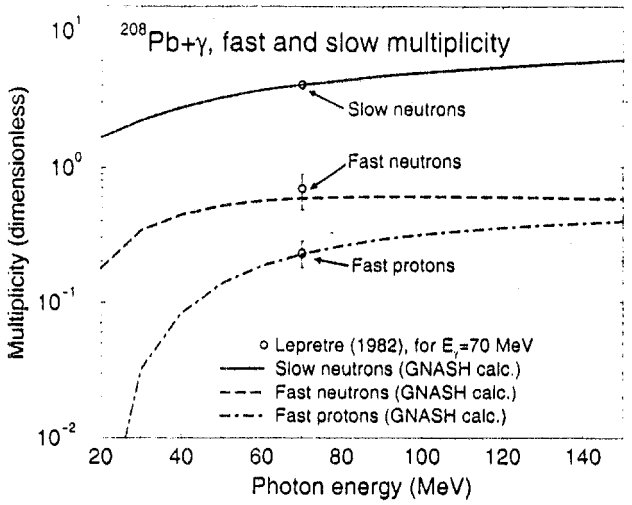

FIG. 3. Evaluated γ+^{208}Pb photoneutron and photoproton multiplicities, based on GNASH code calculations, compared with measurements. For the photoneutrons, experimental data at 70 MeV have been separated into fast (preequilibrium) and slow (equilibrium) contributions, whilst for photoprotons just the fast (preequilibrium) multiplicity is available.

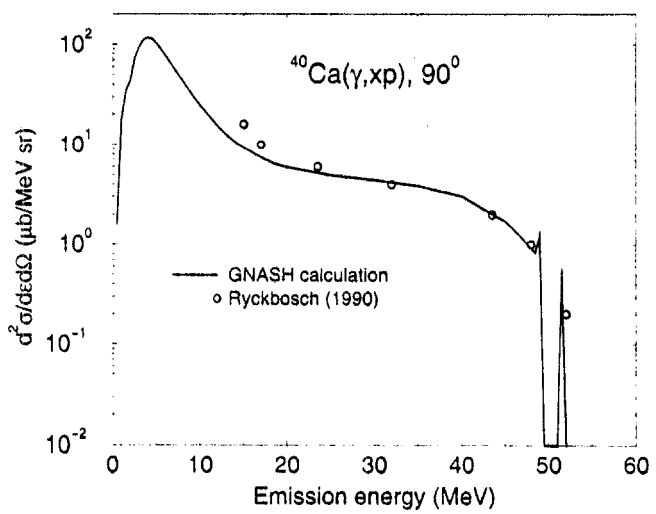

FIG. 4. Calculated inclusive proton emission spectrum for 60 MeV photons on calcium, ^{40}Ca(γ, xp), compared with measurements of Ryckbosch.

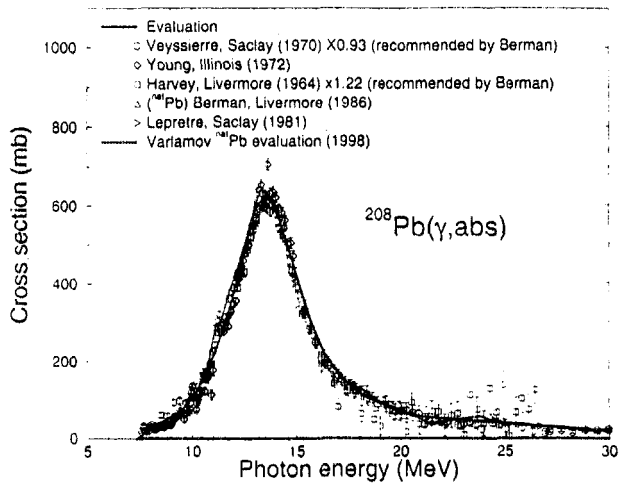

FIG. 5. Evaluated photonuclear absorption cross section for ^{208}Pb as a function of incident photon energy.

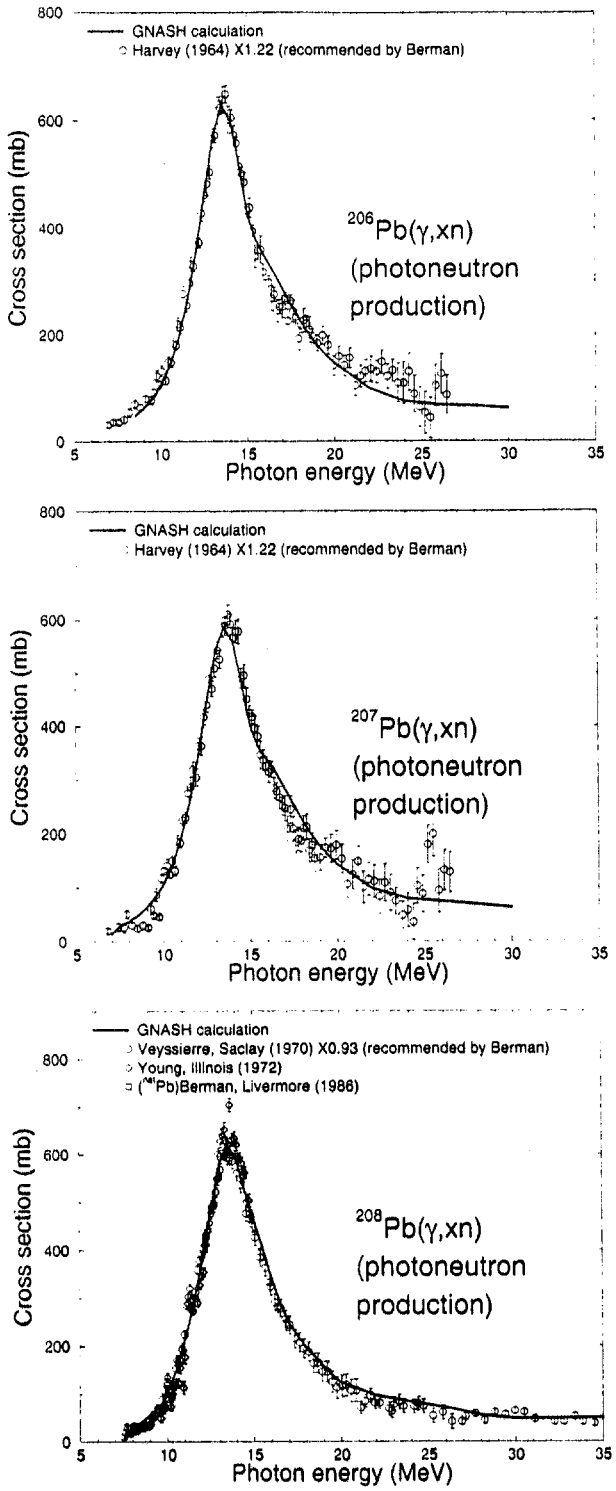

FIG. 6. Evaluated photoneutron production cross section from GNASH calculations for ^{206,7,8}Pb as a function of incident photon energy.

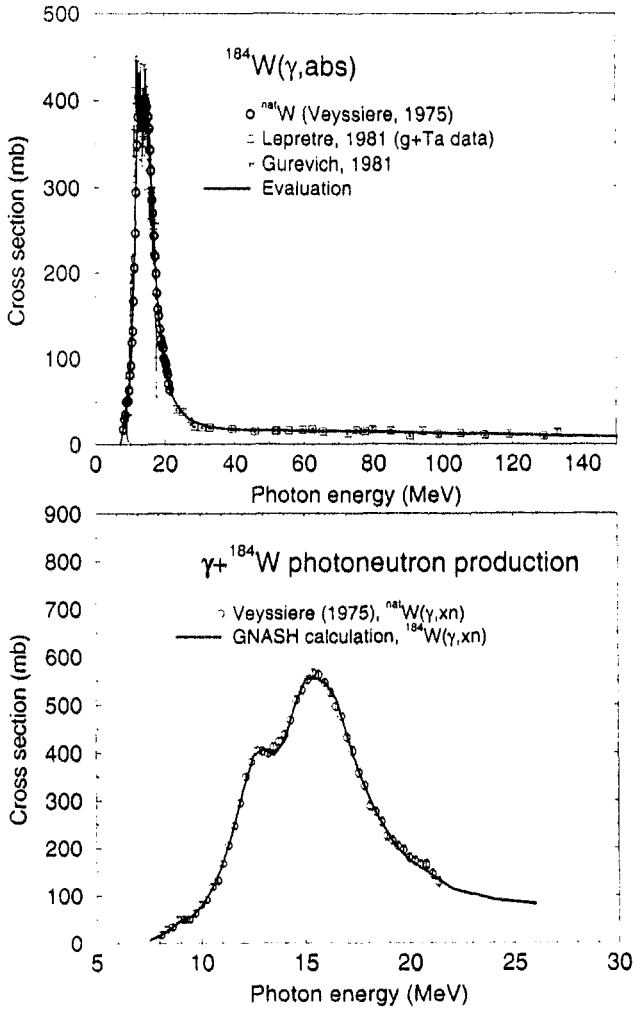

FIG. 7. (a) *Upper graph:* Evaluated photonuclear absorption cross section for ^{184}W as a function of incident photon energy; (b) *Lower graph:* Evaluated photoneutron production cross section from GNASH calculations for ^{184}W as a function of incident photon energy.

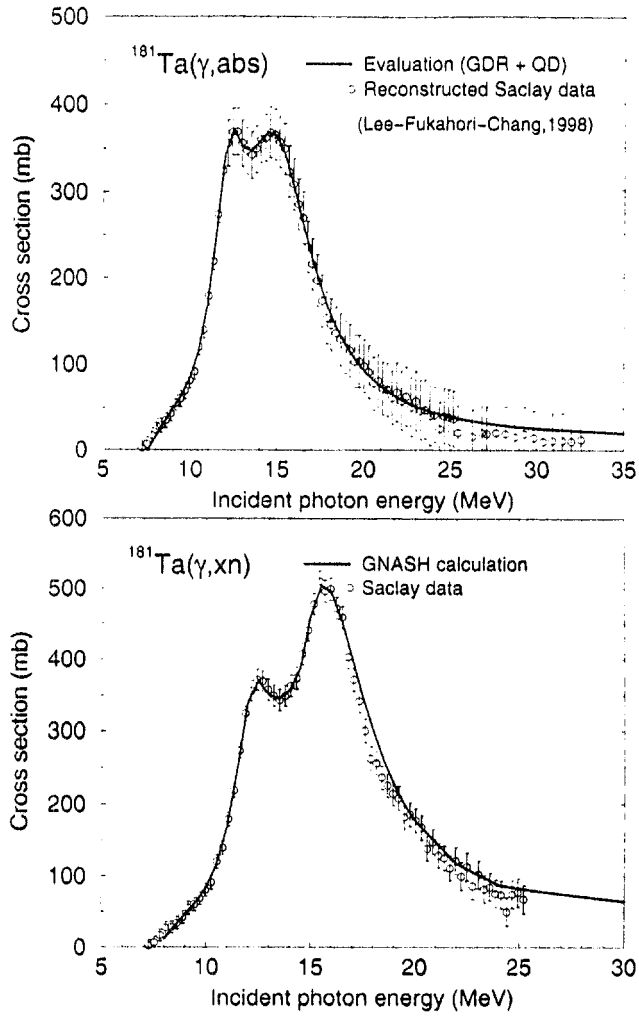

FIG. 8. (a) *Upper graph:* Evaluated photonuclear absorption cross section for ^{181}Ta as a function of incident photon energy; (b) *Lower graph:* Evaluated photoneutron production cross section from GNASH calculations for ^{181}Ta as a function of incident photon energy.

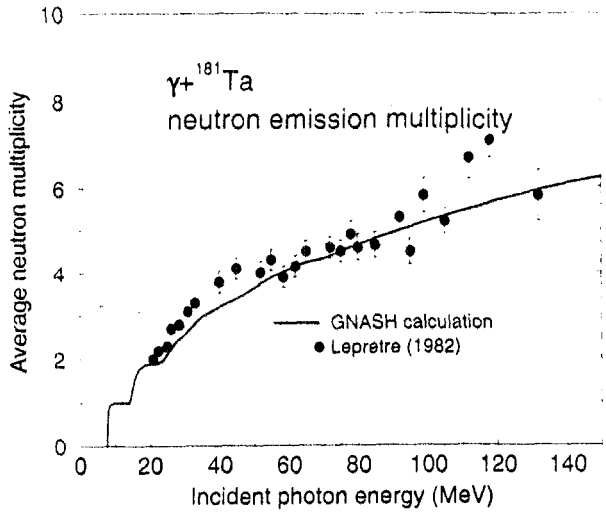

FIG. 9. Calculated neutron emission multiplicity for photons incident on ^{181}Ta as a function of incident photon energy up to 150 MeV.

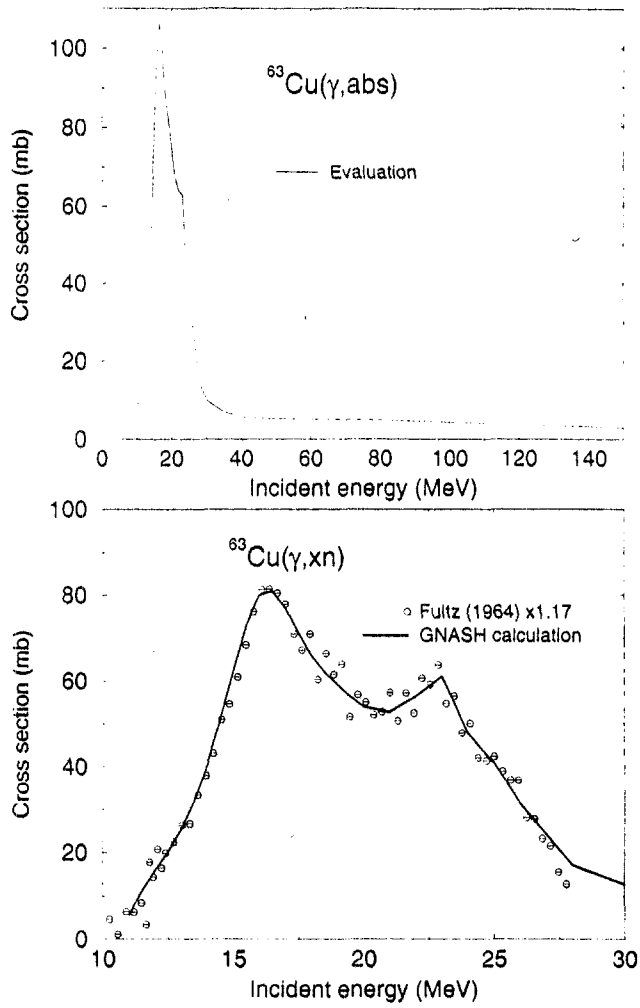

FIG. 10. (a) *Upper graph:* Evaluated photonuclear absorption cross section for ^{63}Ta as a function of incident photon energy; (b) *Lower graph:* Evaluated photoneutron production cross section from GNASH calculations for ^{63}Cu as a function of incident photon energy. Since no measurements exist for the absorption cross section, the evaluated absorption values were chosen so as to result in good agreement between the calculated neutron production cross section and measured neutron production.

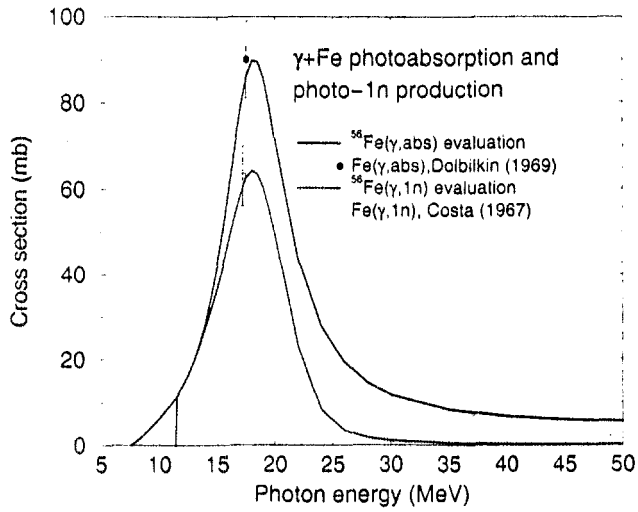

FIG. 11. Evaluated photonuclear absorption cross section and single photoneutron cross section for ^{56}Fe as a function of incident photon energy.

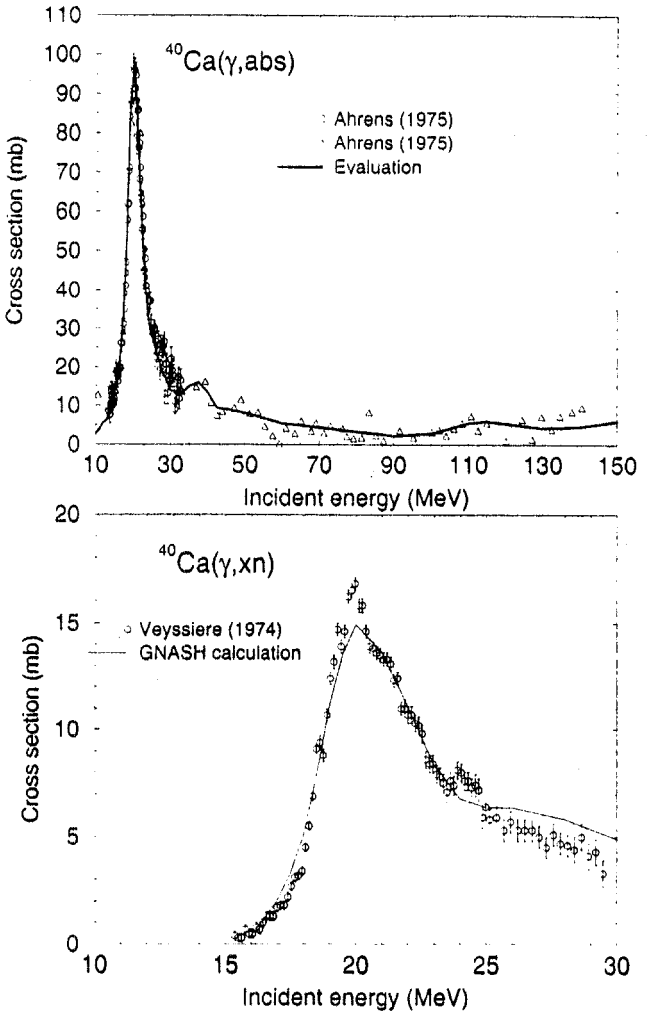

FIG. 12. (a) *Upper graph:* Evaluated photonuclear absorption cross section for ^{40}Ca as a function of incident photon energy; (b) *Lower graph:* Evaluated photoneutron production cross section from GNASH calculations for ^{40}Ca as a function of incident photon energy.

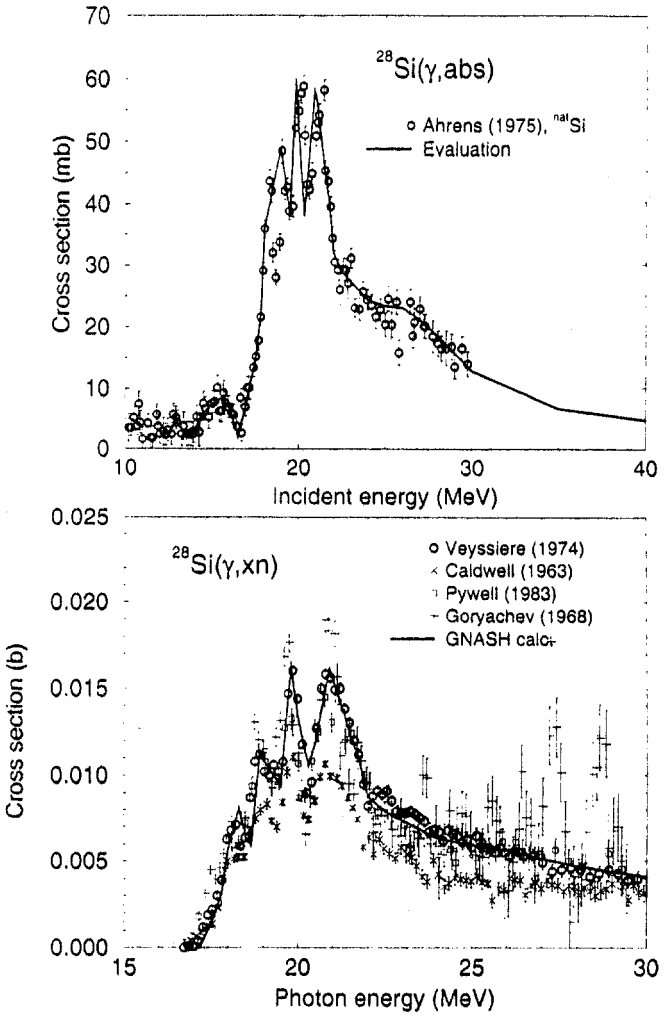

FIG. 13. (a) *Upper graph:* Evaluated photonuclear absorption cross section for ^{28}Si as a function of incident photon energy; (b) *Lower graph:* Evaluated photoneutron production cross section from GNASH calculations for ^{28}Si as a function of incident photon energy.

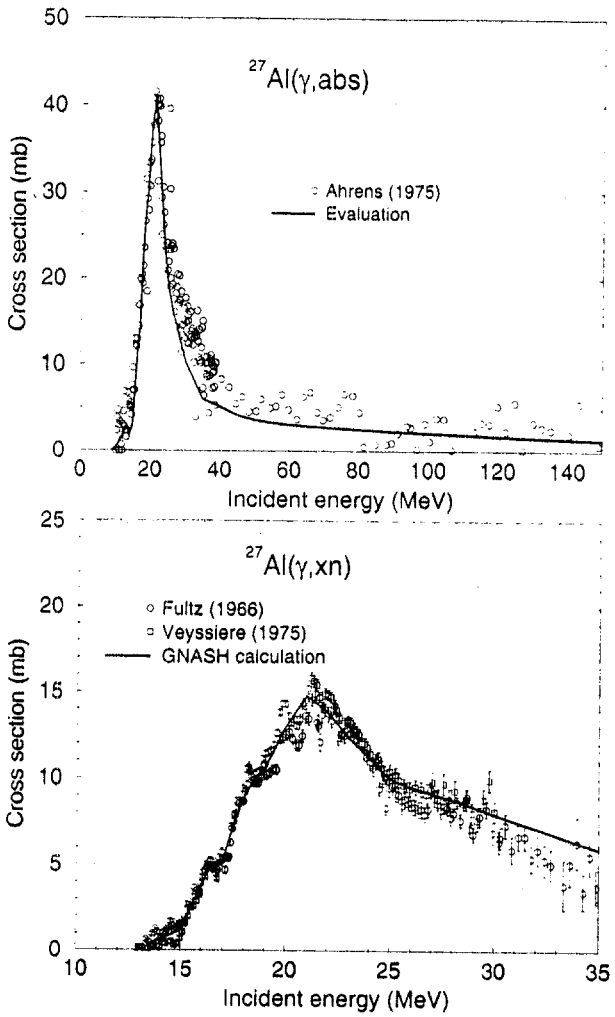

FIG. 14. (a) *Upper graph:* Evaluated photonuclear absorption cross section for ^{27}Al as a function of incident photon energy; (b) *Lower graph:* Evaluated photoneutron production cross section from GNASH calculations for ^{27}Al as a function of incident photon energy.

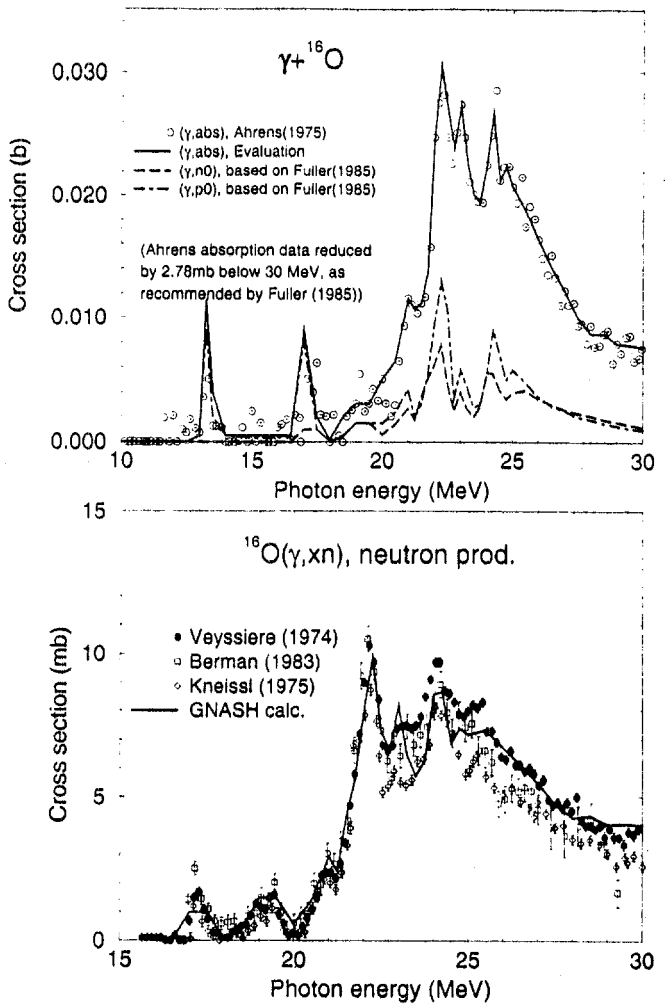

FIG. 15. (a) *Upper graph:* Evaluated photonuclear absorption cross section for ^{16}O as a function of incident photon energy. Also shown are evaluated $(\gamma, n0)$ and $(\gamma, p0)$ cross sections; (b) *Lower graph:* Evaluated photoneutron production cross section from GNASH calculations for ^{16}O as a function of incident photon energy.

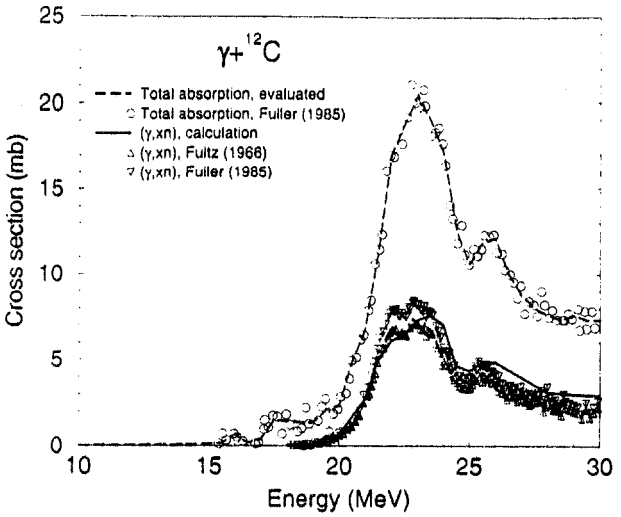

FIG. 16. Evaluated carbon (γ, abs) cross section, and calculated carbon (γ, xn) cross section, compared with measurements.

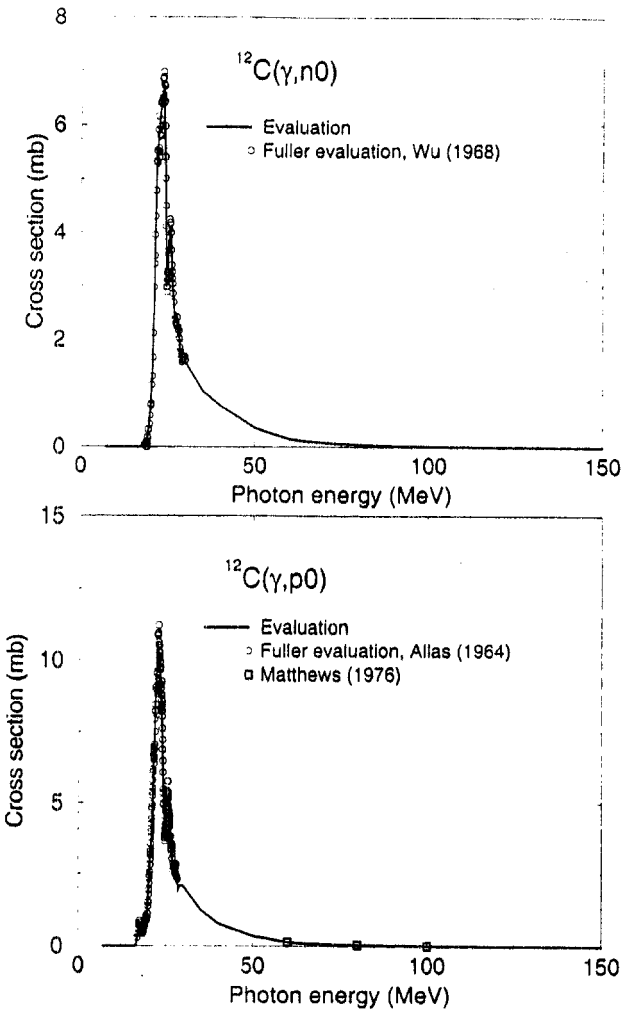

FIG. 17. (a) *Upper graph:* Evaluated carbon $(\gamma, n0)$ cross section; (b) *Lower graph* Evaluated carbon $(\gamma, p0)$ cross section.